

Manipulation of a single charge in a double quantum dot

J. R. Petta, A. C. Johnson, and C. M. Marcus

Department of Physics, Harvard University, Cambridge, MA 02138

M. P. Hanson and A. C. Gossard

Materials Department, University of California, Santa Barbara, California 93106

(Dated: February 2, 2008)

We manipulate a single electron in a fully tunable double quantum dot using microwave excitation. Under resonant conditions, microwaves drive transitions between the (1,0) and (0,1) charge states of the double dot. Local quantum point contact charge detectors enable a direct measurement of the photon-induced change in occupancy of the charge states. From charge sensing measurements, we find $T_1 \sim 16$ ns and a lower bound estimate for T_2^* of 400 ps for the charge two-level system.

PACS numbers: 73.21.La, 73.23.Hk, 85.35.Gv

Mesoscopic circuits can be designed to create artificial two-level systems that can be controlled on nanosecond time scales, allowing the observation of coherent oscillations between the two quantum states [1, 2]. A broad range of experiments have demonstrated control over the flux states of a SQUID [3], the phase of a Josephson-junction qubit [4, 5], and the charge states of semiconducting quantum dots [6].

Semiconducting quantum dots are promising systems for the manipulation of a single charge because of the relative ease of controlled confinement using electrostatic gates [7, 8]. By this same approach, coupled quantum dots can be used to create two-level systems with precise and rapid control of the coupling between quantum states [9]. Careful control of the interdot tunnel coupling makes it possible to tune from a weakly coupled regime, where a single charge is localized on one of the dots, to a strongly coupled regime, where the charge becomes delocalized [10]. Under resonant conditions, microwaves can induce transitions between the charge states, resulting in controlled charge state repopulation [11, 12, 13].

In this Letter, we create a two-level system from a double quantum dot containing a single electron. We drive resonant transitions between the charge states through the application of microwaves. Previously, photon assisted tunneling (PAT) has been used to detect microwave excitation of a many-electron double quantum dot [10]. Here we directly measure the occupancy of the charge states using local quantum point contact (QPC) charge detectors [14]. From these measurements we have extracted the lifetimes T_1 and T_2^* for a semiconductor dot based charge two-level system [15]. In contrast with PAT, which requires coupling to the leads, our sensing technique can be used in regimes where transport is not possible, allowing for spectroscopy of an isolated double dot.

Measurements are performed on gate-defined quantum dots fabricated on a GaAs/Al_{0.3}Ga_{0.7}As heterostructure grown by molecular beam epitaxy (Fig. 1(a)). A two-dimensional electron gas with electron density $2 \times 10^{11} \text{ cm}^{-2}$ and mobility $2 \times 10^5 \text{ cm}^2/\text{V}\cdot\text{s}$ lies 100 nm below the surface and is depleted with Ti/Au top gates.

Gates 2–6 and t form the double quantum dot. Gates 3–5 are connected via bias tees to dc and microwave sources [16]. QPC charge detectors are created by depleting gates 1 and 7, while gate 8 is energized to isolate the QPC sensor from the double dot circuitry. Gates 9–11 are unused.

The double dot conductance, G_D , and the QPC conductances, $G_{S1(S2)}$, are measured using standard ac lock-in techniques with the sample cooled to base temperature in a dilution refrigerator. The electron temperature, $T_e \sim 135$ mK, was determined from Coulomb blockade peak widths. The double dot is voltage biased with a $6 \mu\text{V}$ excitation at 17 Hz, while the QPC detectors are current biased at 1 nA at frequencies of 93 and 97 Hz.

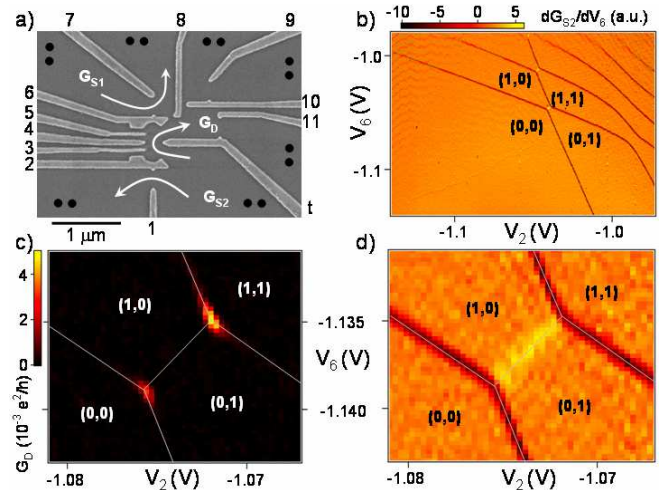


FIG. 1: (a) SEM image of a device identical in design to the one used in this experiment. Gates 2–6 and t define the double dot. QPC charge detectors are formed by depleting gates 1 and 7. Gate 8 may be used to separate the QPC and double dot conductance measurement circuits. Gates 9–11 are not energized. • denotes an ohmic contact. (b) Large scale plot of dG_{S2}/dV_6 as a function of V_2 and V_6 . Charge states are labelled (M, N) , where $M(N)$ is the time averaged number of electrons on the upper (lower) dot. G_D , in (c), and dG_{S2}/dV_6 , in (d), as a function of V_2 and V_6 near the $(1,0)$ to $(0,1)$ transition. In (c–d) the gates have been slightly adjusted relative to (b) to allow simultaneous transport and sensing. Identical color-scales are used in (b) and (d).

This setup allows a simultaneous measurement of G_D , G_{S1} , and G_{S2} .

Transport in the few-electron regime is made difficult by the reduction in tunnel coupling to the leads as the dot is depleted [7]. However, recent experiments using both charge sensing and transport have shown that it is possible to create a few electron double dot without sacrificing transport [17]. We demonstrate similar control in Fig. 1 (b–d). Figure 1(b) shows dG_{S2}/dV_6 (numerically differentiated) as a function of V_2 and V_6 . Electrons entering or leaving the double dot, or moving from one dot to the other, change the QPC conductance. These changes show up clearly in the gate voltage derivatives of G_{S1} and G_{S2} , and directly map out the charge stability diagram of the double dot. The nearly vertical lines correspond to charge transitions in the lower dot, while the nearly horizontal lines are due to charge transitions in the upper dot. In the lower left corner of the charge stability diagram, the double dot is completely empty, denoted (0,0). With the device configured as in Fig. 1(b), the transport signal near the (1,0) to (0,1) transition is below the noise floor of the measurement. A slight retuning of the gates results in transport. Figure 1(c) shows a color scale plot of G_D near the (1,0) to (0,1) charge transition. A simultaneously acquired charge stability diagram is shown in Fig. 1(d). In the remainder of the paper, we will focus on the (1,0) to (0,1) charge transition. Crossing this transition by making V_6 more positive transfers a single electron from the lower dot to the upper dot. This increases G_{S2} , resulting in the yellow line in the charge stability diagram. In contrast, the dark lines correspond to charge transitions that increase the total number of electrons on the double dot as V_6 is increased, resulting in a decrease in G_{S2} .

Near the interdot transition, the double dot forms a two-level charge system that can be characterized by the detuning parameter, ϵ , and the tunnel coupling, t (see inset of Fig. 3(d)) [9]. Tuning t controls the crossover from localized to delocalized charge states [10]. This tunability is important, because proposals involving the manipulation of electron spin in a double dot often require control of the exchange interaction, $J=4t^2/U$ [18]. We demonstrate control of t in the one-electron regime in Fig. 2. As V_t is increased, the interdot charge transition smears out due to the onset of charge delocalization (compare the upper and lower insets). A quantitative measure of t is made by measuring the QPC response along the detuning diagonal (a typical detuning sweep is indicated by the black line in the lower inset of Fig. 2). The QPC response is converted into units of charge following DiCarlo *et al.* [19]. Figure 2 shows M as a function of ϵ for several values of V_t . We fit the experimental data using [19]:

$$M = \frac{1}{2} \left(1 - \frac{\epsilon}{\sqrt{\epsilon^2 + 4t^2}} \tanh \left(\frac{\sqrt{\epsilon^2 + 4t^2}}{2k_B T_e} \right) \right) \quad (1)$$

where t is a free parameter and k_B is Boltzman's constant. ϵ is converted into units of energy by multiplying

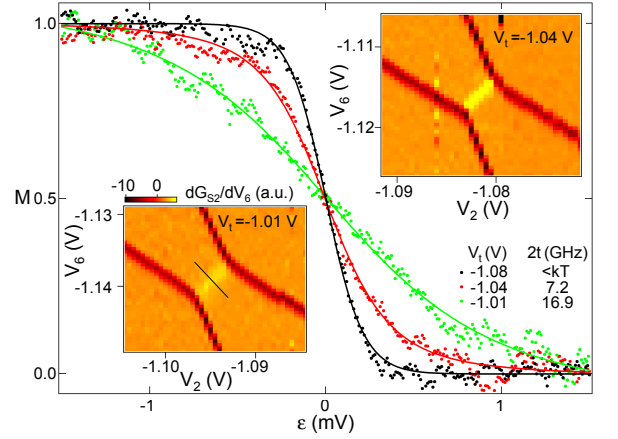


FIG. 2: The number of electrons on the upper dot, M , as a function of detuning, ϵ , for several values of V_t . Solid lines are best fits to the data (see text). Increasing V_t strengthens the interdot tunnel coupling and broadens the interdot charge transition. A typical detuning sweep follows the black line in the lower inset. Insets: Plots of dG_{S2}/dV_6 as a function of V_2 and V_6 for $V_t = -1.01$ V (lower inset) and $V_t = -1.04$ V (upper inset). The same color-scale is used in both insets.

by the lever arm (which takes into account capacitive division of voltage). With $V_t = -1.08$ V, the QPC response is temperature broadened, which places an upper limit on $2t$ of 5.6 GHz. A 30 mV increase in V_t more than doubles t (see the table in Fig. 2).

Microwaves can induce a current at zero source-drain bias when the photon frequency is equal to the energy separation between the (1,0) and (0,1) charge states [20, 21, 22]. This PAT current is shown in Fig. 3(a) as a function of V_2 and V_6 with 24 GHz continuous-wave (cw) applied to gate 4 of the device and $V_{sd} = 0$ μ V. Four sharp resonances appear in the vicinity of each triple point. The resonances closest to each triple point correspond to 1 photon (1γ) processes, while the outer resonances correspond to 2γ processes, consistent with previous observations of PAT in a semiconductor double dot [10, 17].

Charge sensing allows a direct measurement of microwave-induced charge state repopulation [3, 15]. Fig. 3(b) shows a color-scale plot of δG_{S1} as a function of V_2 and V_6 with 24 GHz cw applied to gate 4 of the device and $V_{sd} = 0$ μ V. Four stripes, aligned parallel to the (1,0) to (0,1) charge transition line, appear in the presence of microwaves. These features are absent when no microwave power is applied (Fig. 1(d)). We associate these features with 1γ and 2γ processes that drive an electron from the (1,0) ground state (for negative ϵ) into the (0,1) excited state, or vice versa.

Measurements of the frequency dependence of the resonance confirm that these features are due to a microwave induced repopulation of charge states. The black curve in Fig. 3(c) shows the measured charge on the upper dot, M , as a function of ϵ , in the absence of microwave excitation. Application of microwaves to gate 4 results in resonant peaks in M vs. ϵ that move to larger $|\epsilon|$ with increasing frequency. A detailed measurement of the resonant peak

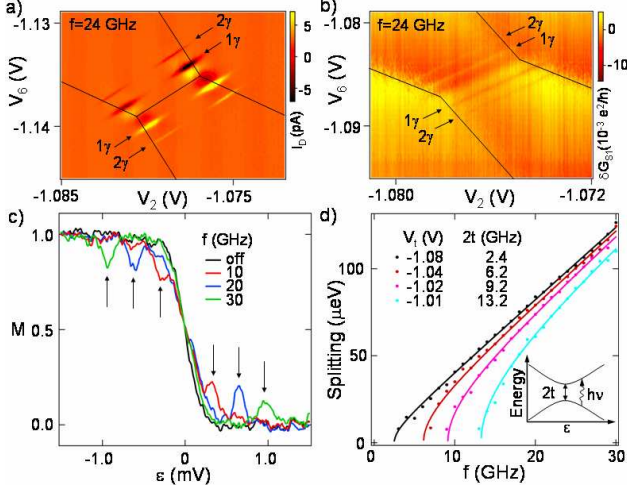


FIG. 3: (a) I_D as a function of V_2 and V_6 with $V_{sd}=0$ μ V. 24 GHz photons are applied to gate 4. Single and two photon processes are visible. Charge transitions are marked with black lines. (b) δG_{S1} as a function of V_2 and V_6 with 24 GHz photons applied to gate 4. A best-fit plane has been subtracted from the data. (c) Number of electrons on the upper dot, M , as a function of ϵ for several microwave frequencies. (d) One-half of the resonance peak splitting as a function of f for several values of V_t . Solid lines are best fit theory curves. Inset: two-level system energy level diagram. The interdot tunnel coupling t results in a splitting of $2t$ at $\epsilon=0$.

position as a function of microwave frequency, f , is used to extract t for various V_t (see Fig. 3(d)) [10]. The peak positions depend linearly on f at high frequency. At low f , the interdot tunnel coupling modifies the linear dependence. The x-axis intercept gives the value of $2t$. For each value of V_t , the experimental data have been fit using $\alpha\epsilon = \sqrt{(hf)^2 - (2t)^2}$, where α is the lever arm. α and t were free parameters for each curve, and α only changes by $\sim 20\%$ over the range of V_t used in Fig. 3. The best fit for $V_t = -1.08$ V is $\alpha = 0.13 \pm 0.02$, consistent with the lever arms obtained by measuring the QPC response as a function of ϵ at higher temperatures [19]. The data in Fig. 3(d) have been converted to energy using the best fit values of α . Our experimental data are well fit by theory and show a variation in t of roughly a factor of 6. In addition, the t values in Fig. 3(d) agree to within 25% with the t values obtained from the data in Fig. 2 using Eq. 1 [19]. The slight discrepancy in the $2t$ values for $V_t = -1.01$ V is due to error in extracting the lever arm for the data in Fig. 2 from temperature scans [23].

The resonant response of a two-level system can be used to extract information about the charge relaxation and decoherence times, as used, for instance, in the recent analysis of the Cooper pair box [15]. Measurements of the resonance peak height as a function of time after the system is moved out of resonance and measurements of the peak width can be used to determine the charge relaxation time T_1 and the inhomogeneous charge decoherence time T_2^* [24].

To measure T_1 the resonance peak height is measured as microwaves are chopped at varying periods, τ , with

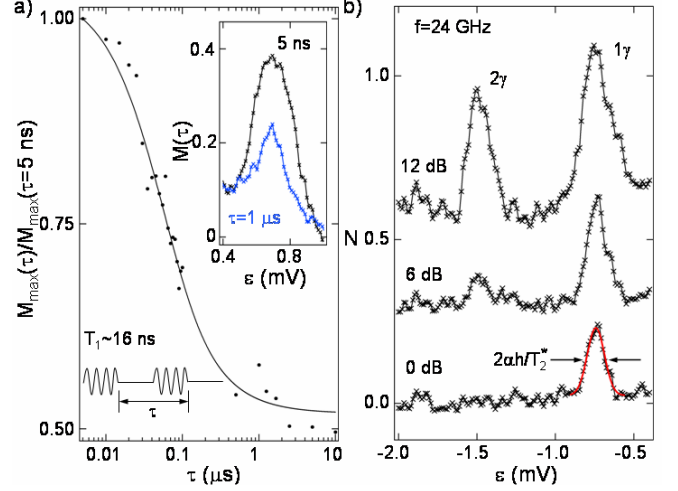


FIG. 4: (a) Resonance amplitude, expressed as $M_{max}(\tau)/M_{max}(\tau=5 \text{ ns})$, as a function of chopped period, τ , with $f=19$ GHz. Theory gives a best fit $T_1=16$ ns (solid line, see text). Inset: 1γ peak shown in a plot of M as a function of ϵ for $\tau=5$ ns and 1μ s. (b) Power dependence of the resonance for $f=24$ GHz. Multiple photon processes occur at higher powers. Curves are offset by 0.3 for clarity.

a 50% duty cycle using a fast mixer circuit [25]. We model the system response with a saturated signal while microwaves are present, followed by an exponential decay with a characteristic time scale T_1 when the microwaves are turned off. Taking the time average, we expect:

$$\frac{M_{max}(\tau)}{M_{max}(0)} = \frac{1}{2} + \frac{T_1(1 - e^{-\tau/(2T_1)})}{\tau} \quad (2)$$

For $\tau \gg T_1$, the exponential tail due to the finite relaxation time represents an insignificant part of the duty cycle, and the QPC detectors measure the time average of the on/off signal, giving a resonant feature with half the height found in the limit $\tau \rightarrow 0$. For very short periods, such that $\tau \ll T_1$, the charge has little time to relax, and the QPC response is close to saturation (saturation is defined as $M_{max}=0.5$ on resonance). When $\tau \sim T_1$, the QPC signal is strongly dependent on τ . To avoid artifacts due to the finite rise time of the mixer circuit, we present data for $\tau \geq 5$ ns. In Fig. 4(a), we plot $M_{max}(\tau)/M_{max}(\tau=5 \text{ ns})$ as a function of τ . The experimental response is in good agreement with this theory, and gives a best fit $T_1=16$ ns.

A measure of the charge decoherence time can be extracted from the resonance peak width. The charge sensor response is an ensemble measurement (in time), so we associate the peak width with the inhomogeneous decoherence time, T_2^* [15, 24]. In Fig. 4(b) we plot N as a function of ϵ for increasing microwave powers. At low power, only the 1γ peak is visible. As the power is increased the 1γ peak approaches saturation and a 2γ peak develops [26]. A Gaussian fit to the low power 1γ peak is shown in red in Fig. 4(b). We find a half-width of 0.077 mV, which corresponds to an energy of 10.2 μ eV when taking into account the lever arm. Converting this into

a time results in a lower bound $T_2^*=400$ ps. The measurement of T_2^* is sensitive to charge fluctuations, which will broaden the resonant feature, resulting in a smaller value for the decoherence time. Thus our measured T_2^* is a worst-case estimate.

We can compare the results of our T_1 and T_2^* analysis with other recent experiments [6, 27]. Fujisawa *et al.* [27] have measured the energy relaxation time in a vertical quantum dot using a pulsed gate experiment. From a measurement of the transient current as a function of pulse time they extract $T_1=10$ ns, which is limited by spontaneous emission of a phonon. The T_2 time of a charge state in a many electron ($N\sim 25$) double dot has recently been measured by Hayashi *et al.* [6]. From the envelope of the decay of Rabi oscillations as a function of time Hayashi *et al.* extract a T_2 time on the order of 1 ns, which serves as an upper bound estimate for T_2^* . The T_1 and T_2^* values that we obtain from charge sensing are in good agreement with the results of these previous experiments.

In conclusion, we have used QPC charge sensing to detect microwave manipulation of a single electron in a double quantum dot. Analysis of the resonance position as a function of frequency allows us to extract the inter-

dot tunnel coupling. Since this method does not rely on transport, it may be used to determine the interdot tunnel coupling when the double dot is completely isolated from the leads. Time-domain experiments and measured line-widths allow us to extract $T_1=16$ ns and $T_2^*=400$ ps for the charge two-level system. In addition, we have demonstrated tunability of t in the few-electron regime, which is a crucial element for many spin manipulation proposals based on fast control of the exchange interaction.

Acknowledgments

We acknowledge useful discussions with Amir Yacoby, Leo DiCarlo, Jacob Taylor, and Mikhail Lukin. Dominik Zumbühl, James Williams, and Abram Falk provided experimental assistance. We thank M. H. Devoret, R. J. Schoelkopf, and their research groups for very useful advice concerning microwave techniques. This work was supported by the ARO under DAAD55-98-1-0270 and DAAD19-02-1-0070, DARPA under the QuIST program, the NSF under DMR-0072777 and the Harvard NSEC.

-
- [1] D. Vion *et al.*, Science **296**, 886 (2002).
 - [2] Y. Nakamura *et al.*, Nature, **398**, 786 (1999).
 - [3] C. H. van der Wal *et al.*, Science **2000**, 290 (2000).
 - [4] Y. Yu *et al.*, Science, **296**, 889 (2002).
 - [5] J. M. Martinis *et al.*, Phys. Rev. Lett., **89**, 117901 (2002).
 - [6] T. Hayashi *et al.*, Phys. Rev. Lett., **91**, 226804 (2003).
 - [7] M. Ciorga *et al.*, Phys. Rev. B, **61**, 16315 (2000).
 - [8] L. P. Kouwenhoven, D. G. Austing, S. Tarucha, Rep. Prog. Phys., **64**, 701 (2001).
 - [9] W. G. van der Wiel *et al.*, Rev. Mod. Phys. **75**, 1 (2003).
 - [10] T. H. Oosterkamp *et al.*, Nature **395**, 873 (1998).
 - [11] P. K. Tien and J. R. Gordon, Phys. Rev. **129**, 647 (1963).
 - [12] L. P. Kouwenhoven *et al.*, Phys. Rev. Lett. **73**, 3443 (1994).
 - [13] T. Fujisawa and S. Tarucha, Superlatt. Microstruct. **21**, 247 (1997).
 - [14] M. Field *et al.*, Phys. Rev. Lett. **70**, 1311 (1993).
 - [15] K. W. Lehnert *et al.*, Phys. Rev. Lett. **90**, 027002 (2003).
 - [16] Anritsu Company, Model K251.
 - [17] J. M. Elzerman *et al.*, Phys. Rev. B **67**, 161308 (2003).
 - [18] D. Loss and D. P. DiVincenzo, Phys. Rev. A **57**, 120 (1998).
 - [19] L. DiCarlo *et al.*, Phys. Rev. Lett. **92** 226801 (2004).
 - [20] C. A. Stafford and N. S. Wingreen, Phys. Rev. Lett. **76**, 1916 (1996).
 - [21] T. H. Stoof and Y. V. Nazarov, Phys. Rev. B **53**, 1050 (1996).
 - [22] P. Brune, C. Bruder, H. Schoeller, Phys. Rev. B **56**, 4730 (1997).
 - [23] The lever arms for the data in Fig. 2 are determined by increasing temperature until the charge transition is thermally broadened. Increased charge noise at higher temperatures resulted in $\sim 20\%$ error in the lever arm for the $V_t=-1.01$ data in Fig. 2.
 - [24] A. Abragam, *The Principles of Nuclear Magnetism: The International Series of Monographs on Physics 32* (Oxford University Press, Oxford, 1983).
 - [25] Marki Microwave, Model MM8-0420MS-00.
 - [26] We have occasionally observed peak heights exceeding saturation, implying microwave induced population inversion. (Petta, Johnson, Marcus, Hanson, Gossard) unpublished.
 - [27] T. Fujisawa *et al.*, Nature, **419**, 278 (2002).